RSC Advances

PAPER

View Article Online
View Journal | View Issue

Check for updates

Cite this: *RSC Adv.*, 2020, **10**, 33112

Highly conductive and transient tracks based on silver flakes and a polyvinyl pyrrolidone composite†

Su Ding, * Qingfeng Cai, Jintao Mao, Fei Chen, Li Fu, Yanfei Lv and Shichao Zhao*

Received 30th July 2020
Accepted 10th August 2020

DOI: 10.1039/d0ra06603f

rsc.li/rsc-advances

Transient electronics have been widely researched to solve the electronic waste (E-waste) issue. Although various transient materials and devices have been reported, the fabrication technique for transient conductors always uses expensive sputtering or evaporation processes. In this study, a silver flake (AgF) and polyvinyl pyrrolidone (PVP) composite is prepared for conductive and transient tracks. The AgF/PVP composite tracks are highly conductive with a resistivity of 8.9 mOhm cm after sintering at 80 °C for only 3 minutes. Impressively, the AgF/PVP tracks disintegrate in water in 3 minutes due to the fast dissolution of the water-soluble PVP. The transient behavior of the AgF/PVP tracks has potential in transient electronics as demonstrated in a light emitting diode (LED) circuit and antenna.

Open Access Article. Published on 07 September 2020. Downloaded on 2/9/2026 7:46:54 PM.
This article is licensed under a Creative Commons Attribution-NonCommercial 3.0 Unported Licence.

1 Introduction

Transient electronics can potentially suppress the electronic waste (E-waste) pollution, caused by the rapid development of consumer electronics, including phones, computers, and electric appliances.[1–6] Normally, E-waste is disposed of *via* several methods, including dissolution in strong acids, burning and landfilling, all of which migrate chemical products into the receiving waters and food chains.[1,7–9] Such processing is harmful to the environment and human health. In contrast, transient electronics are designed to operate for a certain duration and then self-deconstruct in water after finishing the task.[10–13] Thus, transient devices are highly desirable for applications in zero-waste electronics, biomedical implant devices, and secure electronics.[5,10,14–17]

Metals, which are essential in electrical devices, are used to form a conductive pattern on the printed circuit boards and as a connection material for the assembly of functional components.[18–20] The waste of electric and electronic equipment (WEEE) consist of more than 60% metals, which are generally recycled by acid leaching and precipitative routes for economic reasons.[21,22] Rogers group[23] first reported the integration of silicon-based transient electronics using magnesium (Mg) for interconnections due to its excellent conductivity, rapid rate of hydrolysis and biocompatibility. The results show that the Mg trace (150 nm) was diffused in water after 3 hours, a duration much longer than that of soluble polymer substrates (normally in minutes).[3,6] Subsequently, reactive dissolution of thin films of Mg alloy, Zn, Fe, W, and Mo in water is systematically studied to assess the potential applications in transient electronics. The dissolution of these thin films normally takes one week to several months and involves the fast degradation of the base metal and the disappearance of the residual oxides.[24] The low dissolution rate of metals prolongs the transient duration of electronics. Additionally, the fabrication of thin metallic films always employs complex electron beam evaporation, magnetron sputtering or lithography techniques. Development of simple and scalable techniques is expected to fabricate transient conductors with short dissolution durations.

Organo–inorganic nanocomposites are promising in various fields, including photocatalysis, energy storage, capacitor, conductor, *etc*[25–29]. Incorporating functional moieties on nanomaterials offers a way to tailor the comprehensive performance of the composition.[30–36] Huang's group[9] reported a simple fabrication of Ag nanowire (AgNW) conductor on soluble polymer substrate as both electrodes of a transient alternating current electroluminescent (ACEL) device. The fabricated ACEL device can be thoroughly dissolved in water within 30 min. The AgNW and polymer composite conductor combines the advantages of both the metallic Ag and soluble polymer providing new method to fabricate transient conductors. In this paper, we fabricate silver flake (AgF) and polyvinyl pyrrolidone (PVP) conductive tracks and examine their potential for use in transient electronics. The raw material of AgFs in the as-prepared AgF/PVP conductive tracks is conveniently recyclable after dissolution in water and thus, superior to the conventional acid washing process used to recycle precious metals, such as Cu and Au. The AgF/PVP composite tracks sintered at 80 °C for 3 minutes show good electrical performance and transient behavior. The AgF/PVP composite track is successfully applied in a light emitting diode (LED) transient circuit, thus, demonstrating its potential use in more complex transient electronics.

College of Materials and Environmental Engineering, Hangzhou Dianzi University, 310018 Hangzhou, P. R. China. E-mail: dingsu@hdu.edu.cn; zhaoshichao@hdu.edu.cn

† Electronic supplementary information (ESI) available. See DOI: 10.1039/d0ra06603f

This journal is © The Royal Society of Chemistry 2020

Open Access Article. Published on 07 September 2020. Downloaded on 2/9/2026 7:46:54 PM.
This article is licensed under a Creative Commons Attribution-NonCommercial 3.0 Unported Licence.

2 Experiments

2.1 Fabrication of AgF/PVP conductive tracks

Polyvinylpyrrolidone (PVP, K30, Shanghai Aladdin Bio-Chem Technology Co., LTD, Shanghai, China) and Ag flakes (Bolong Silver Industry, Hunan, China) were used as purchased without further purification. PVP solution (20 wt% in ethanol) was prepared and mixed with AgF powder with different mass ratios to form Ag ink. The Ag ink was ultrasonic vibrated for 5 minutes and stirred by hand for several seconds to achieve homogeneous ink. Then, 80 μL Ag ink was dropped onto a glass substrate with size of 4 × 26 mm controlled by tapes. The ink-coated glass films were heated in an oven at 80 °C for 3 minutes to remove the ethanol. After peeling off the tapes, AgF/PVP conductive tracks were successfully obtained.

2.2 Characterization of the AgF/PVP conductive tracks

The rheology experiments of the AgF/PVP ink were carried out at room temperature using a rotational rheometer (MCR52, Anton Paar). The viscosity properties of the ink were obtained by varying the shear rate from 30 to 500 s^{-1}. The composition of the AgF/PVP conductive tracks were confirmed by X-ray diffraction (XRD, Miniflex600, Rigaku Corporation) and X-ray photoelectron spectroscopy (XPS, K-Alpha, Thermo Fisher Scientific). XRD patterns were recorded at room temperature with scanning speed of 5° min^{-1} from 10° to 80°. XPS results were amended using the C 1s peak at binding energy of 284.6 eV as reference. The morphology of the AgF/PVP conductive tracks was checked by scanning electron microscopy (SEM, Apreo, FEI). The elemental composition of the AgF/PVP track was monitored using the energy dispersive spectroscopy (EDS) equipped on the SEM. The thermal characterization of the AgF/PVP tracks was operated on a TGA/DSC analyzer (TGA/DSC LF1600, Mettler) under a nitrogen ambient atmosphere with a heating rate of 10 °C min^{-1}, from 25 to 800 °C.

2.3 Properties and applications of the AgF/PVP conductive tracks

Resistivity. The thickness of the AgF/PVP conductive tracks was measured under an optical microscope (MV 3000, Nanjing Jiangnan Novel Optics Co., Ltd.). The sheet resistance was examined by four-probe method with a surface resistivity meter (RTS-9, Guangzhou Four-Point Probes Technology Co. Ltd). The resistivity was calculated by multiplying the sheet resistance with the thickness of the track, which was checked by optical microscope. The sheet resistance was collected from at least 3 samples and 3 points were tested for each sample.

Transiency. The transient property of the AgF/PVP conductive tracks was examined by immersing these samples into water to view the evolution of the AgF/PVP tracks. The AgF/PVP conductive track was considered to be failed when the track was partly decomposed or totally fell off the substrate.

Applications. To demonstrate the application of the AgF/PVP transient track in a LED circuit powered by a DC source (KRP-305D, Shenzhen Zhaoxin Electronic Instruments Equipment Co. Ltd), the AgF/PVP track was coated on a printed circuit board (PCB) as a part of the wire and immersed in water. The brightness of the LED was monitored during the whole process. The AgF/PVP ink was further printed on a flexible polyethylene glycol terephthalate (PET) substrate to make a dipole antenna with two poles of size of 75 × 4 mm. A network analyzer (E5971C, Agilent Technologies) was used to measure the return loss of the antenna.

3 Results and discussion

Fig. 1 is a schematic illustration of the experiments. The AgFs are mixed with PVP to form Ag ink, followed by the coating of glass substrates with the Ag ink. After a rapid sintering process, high-performance AgF/PVP tracks are achieved due to the excellent conductivity of AgFs. The AgF/PVP tracks can be readily dissolved in water owing to the addition of water-soluble PVP. The dissolved AgF/PVP composite is disintegrated into dispersed AgFs after tens of seconds of ultrasonic vibration, and can be commodiously recycled during the E-waste disposal process. Compared with the traditional acid leaching procedure, the expensive AgF/PVP conductive tracks can be more conveniently recycled. This proposal put forward a simple and effective strategy for fabricating conductive tracks in transient electronics and should be prioritized in the recycling process in the meantime.

Fig. 1 Schematic illustration of the experimental process of the Ag conductive track.

Open Access Article. Published on 07 September 2020. Downloaded on 2/9/2026 7:46:54 PM.
This article is licensed under a Creative Commons Attribution-NonCommercial 3.0 Unported Licence.

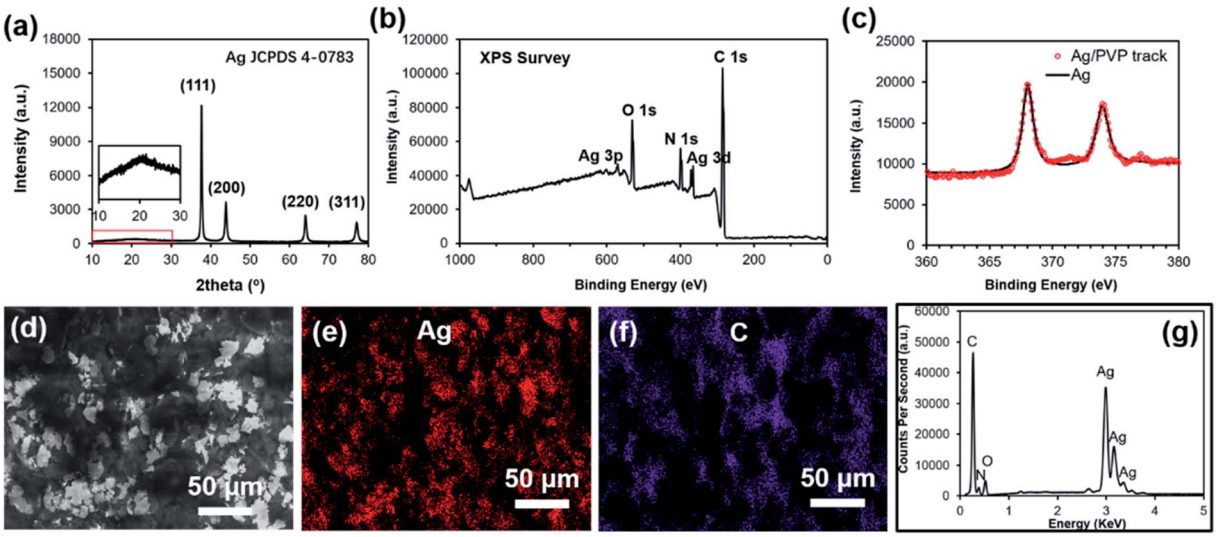

Fig. 2 Composition and morphology characterization of the AgF/PVP composite tracks. (a) XRD pattern, (b) XPS survey spectra and (c) Ag 3d spectra of the AgF/PVP composite track. (d) SEM images of the AgF/PVP conductive tracks. (e and f) EDS images and (g) element spectrum of AgF/PVP conductive tracks in figure (d).

The composition and the morphology of AgF/PVP conductive tracks is examined as shown in Fig. 2. The XRD pattern of the AgF/PVP track with diffraction peaks at 2θ value 38.1°, 44.1°, 64.4° and 77.3° indexes to the {111}, {200}, {220} and {311} planes of Ag (JCPDS 4-0783). The broad band located around 22° corresponds to the amorphous PVP as reported in previous ref. 37. XPS measurement of survey spectra (Fig. 2(b)) shows the presence of C, N, O and Ag signals. High resolved XPS Ag 3d spectra of the AgF/PVP track and standard Ag are presented in Fig. 2(c). The XPS Ag 3d 5/2 and 3d 3/2 binding energies for AgFs appears at 368 and 374 eV, respectively, which is in good agreement with standard Ag values.[38] In addition, there is no XPS peaks of AgO and Ag_2O having binding energies at 367.33 eV and 367.62, respectively.[39] The XRD and XPS results demonstrate the as-prepared tracks comprise Ag and PVP without other impurities. The AgFs are randomly dispersed on the surface and connect with each other in plane or through the 3-dimensional AgF network that is partially embedded in the PVP polymer as shown in Fig. 2(d). The energy-dispersive X-ray spectroscopy (EDS) images reveal the distribution of the AgFs and the PVP polymer on the surface. The Ag and C element mapping coincides with the sites of the grey flakes and the dark polymer in Fig. 2(d), respectively. Although the AgFs are partially separated by the insulated PVP polymer as shown in the EDS images, the AgFs join with other flakes to form conductive paths such that the resistivity of the AgF/PVP composite track is only 8.9 mOhm cm with only 40% AgFs, demonstrating the good connections of the AgFs in the 3-dimensional AgFs network. The conductivity of the AgF/PVP composite track is better than the previously reported values[9,10,23] and can be further improved by adding more AgFs.

To study the effect of the quantity of the AgFs, various AgF/PVP composite tracks with different mass ratios are prepared and the corresponding properties are examined. Fig. S3† illustrate the viscosity curve for the AgF/PVP ink with various AgF concentrations. The steady viscosity is 31.3, 32,3, 32.7 and 34.9

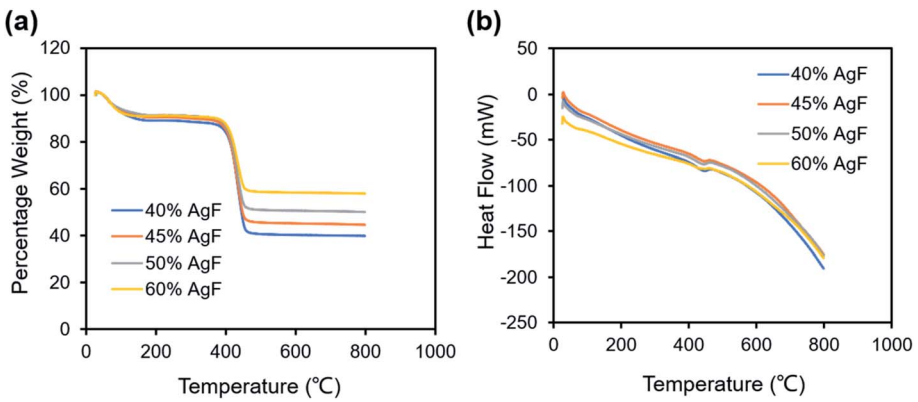

Fig. 3 TGA/DSC result of the AgF/PVP composite.

 This journal is © The Royal Society of Chemistry 2020

Open Access Article. Published on 07 September 2020. Downloaded on 2/9/2026 7:46:54 PM.
This article is licensed under a Creative Commons Attribution-NonCommercial 3.0 Unported Licence.

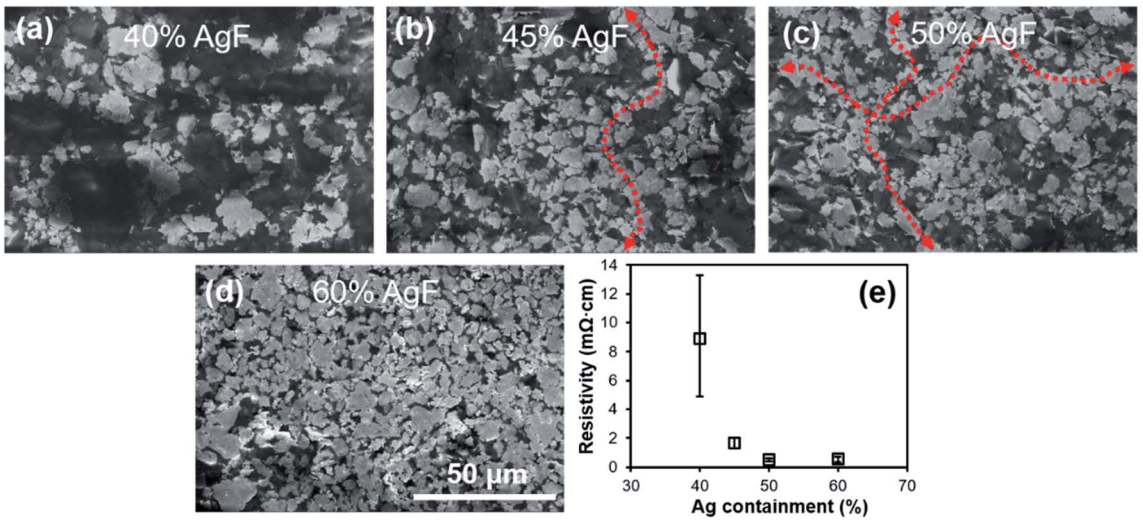

Fig. 4 SEM images (a–d) and resistivity (e) of AgF/PVP conductive tracks with various AgF containments. (a) 40%, (b) 45%, (c) 50%, (d) 60%.

mPa s for the AgF/PVP ink with 40%, 45%, 50% and 60% AgFs, respectively. The results show viscosity increase with increasing Ag concentration. The thermal stability of the AgF/PVP conductive track are characterized by TGA/DSC as shown in Fig. 3. There is a well defined weight loss for all the tracks at 400–460 °C at which temperature the DSC curves show endothermic peaks. The weight loss corresponds to the decomposition of the PVP polymer. The percentage weights are 39.8%, 44.6%, 50.1% and 58.0%, respectively for the AgF/PVP conductive tracks with 40%, 45%, 50% and 60% AgFs containments indicating the residuals are metallic Ag. Fig. 4 shows the morphology and resistivity of the AgF/PVP composite tracks with AgF contents of 40%, 45%, 50% and 60%. The original AgFs are several micrometers in size as presented in Fig. S1.† The AgF/PVP tracks have a smooth surface with AgFs uniformly dispersed in the PVP polymer as shown in Fig. 4. The AgFs inlay in the PVP polymer without discordant interfaces shows good adhesion between AgFs and PVP. When the AgF content is only 40%, the density of the AgFs on the surface of the composite is relatively low, and a small percent of the AgFs connect with each other. With increase in AgF containment (45% and 50%), the density of the AgFs obviously increases such that conductive paths can be formed in plane as marked in Fig. 4(b and c). A dense AgF network is formed with 60 wt% AgFs which helps to improve the conductivity. The resistivity of the AgF/PVP tracks at various mass ratios is given in Fig. 4(e). The resistivity is only 8.9 mOhm cm when 40% AgFs are added in the composite tracks, resulting in excellent electrical performance that is suitable for commercial conductors. The AgF/PVP conductive track also shows a good current carrying capacity (Fig. S4†). When the content of AgFs is imcreased to 45%, the resistance declines to 1.6 mOhm cm. The resistance further decreases to 567 μOhm cm and 510 μOhm cm if the addition of AgFs is improved to 50% and 60%, respectively. This result indicates that the conductivity of the AgF/PVP tracks is obviously improved when more AgFs are mixed in the composite because more conductive paths are built between the AgFs.

The transient behavior of the AgF/PVP composite tracks is examined as displayed in Fig. 5, which shows the sequential images of the dissolution of AgF/PVP tracks with different Ag contents. The AgF/PVP conductive tracks are disintegrated or slip into the water after several minutes or hours depending on the composition of the tracks. The AgF/PVP conductive track with 40% AgFs starts to dissolve after it is placed in water for 1 minute, and some of the AgFs slipped from the glass substrates. An obvious crack is generated in the AgF/PVP

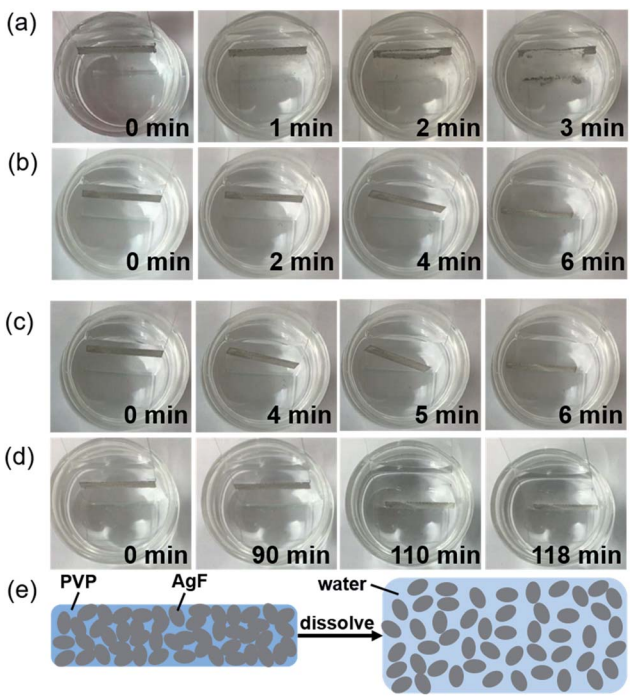

Fig. 5 Sequential images of the dissolution of Ag/PVP tracks with different Ag contents. (a) 40%, (b) 45%, (c) 50%, (d) 60%. (e) Schematic illustration of the dissolution process of the AgF/PVP composite tracks after dropped in water.

Open Access Article. Published on 07 September 2020. Downloaded on 2/9/2026 7:46:54 PM.
This article is licensed under a Creative Commons Attribution-NonCommercial 3.0 Unported Licence.

Table 1 Comparison of electrical properties for our transient conductors and previous works[a]

Materials	Resistance or conductance	Thickness	Dissolving duration	Ref.
W strip	5200 S m^{-1}	40 μm	8 minutes	10
Mg trace	1.04 Ω mm^{-1}	300 nm	3 hours	23
Ag NW transparent electrode	6 Ω sq^{-1}	58%	30 minutes	9
Ag microparticles trace	1.59 Ω sq^{-1}	—	500 seconds	40
AgF/PVP composite track	8.9 mΩ cm	83 μm	180 seconds	Our work

[a] Ag NW represents silver nanowire.

composite track followed by total disintegration in water after 3 minutes. It is concluded that rapid dissolution of the AgF/PVP conductive track occurs due to the addition of water-soluble PVP, which binds the AgFs together to form a highly conductive track and dissolves the AgF clusters after being placed in water (Fig. 5(e)). The excellent electrical performance and transience of the AgF/PVP composite tracks enable potential applications in transient electronics to solve the E-waste issue. When more AgFs are added, the AgF/PVP tracks also fail after several or a hundred minutes as shown in Fig. 5(b–d). The AgF/PVP tracks creep into the water without decomposition because the AgFs are closely piled up with higher AgF contents such that only the surface is uncovered and loose PVP is dissolved in water to destroy the connection of the composite tracks and glass substrates. Although AgFs/PVP composite tracks with higher AgF containment (45%, 50% and 60%) have better conductivity, the failure behavior could cause a short out or program disruption.

The AgF/PVP composite track has a great advantage compared with those previously reported, as shown in Table 1. The conductivity of the AgF/PVP composite track is better than that in other papers, except for the Mg trace, which is prepared by a complex physical deposition method. The dissolution duration of our AgF/PVP composite is shorter than those of other materials. Considering both the conductivity and transient property, the AgF/PVP composite track with 40% AgF content is suitable for application in transient circuits as demonstrated in our experiment (Fig. 6). The AgF/PVP conductive track is printed on a PCB to work as a component of the wire in the LED circuit, and it is immersed into water to view the variations in the brightness of the LED. The brightness of the LED gradually weakens with the dissolution of the AgF/PVP track and finally dies out after 4 minutes when the AgF/PVP track is broken. The application of the AgF/PVP conductive track as further demonstrated, showing that the AgF/PVP ink is printed on a PET substrate to fabricate a dipole antenna device as shown in Fig. 6(b). The resistance of each pole of the AgF/PVP antenna is 4 Ohm, which is relatively high compared with 0.5 Ohm resistance of the pure Ag antenna. The results show that the pure Ag dipole antenna return loss is −22 dB at the design frequency of 900 MHz. In contrast, the return loss of the AgF/PVP antenna at the same frequency is −17 dB, showing a performance similar to that of the pure Ag antenna due to the high conductivity. The excellent performance of the

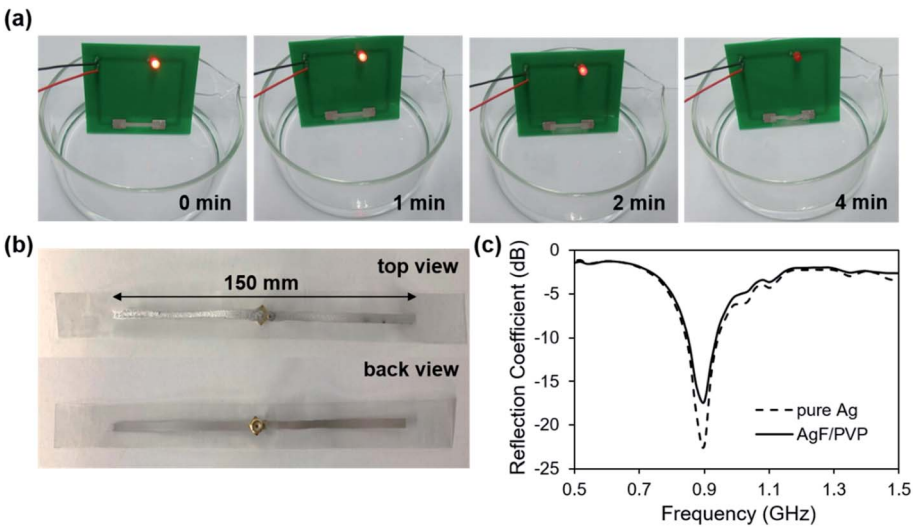

Fig. 6 Applications of the AgF/PVP transient tracks. (a) Sequential dissolution images of Ag/PVP conductive tracks on commercial PCB. (b) Optical image of the dipole antenna made of AgF/PVP conductive track. (c) Comparison of reflection coefficient for the AgF/PVP conductive track dipole antenna (solid) and pure Ag track dipole antenna (dotted).

 This journal is © The Royal Society of Chemistry 2020

Open Access Article. Published on 07 September 2020. Downloaded on 2/9/2026 7:46:54 PM.
This article is licensed under a Creative Commons Attribution-NonCommercial 3.0 Unported Licence.

AgF/PVP transient antenna makes it potentially useful in information transmission and security.

4 Conclusion

In summary, we have proposed a highly conductive and transient track from a composite material of AgFs and PVP which are prepared at 80 °C for 3 minutes. The AgF/PVP composite track with 40% AgF content has an excellent resistivity of 8.9 mOhm cm. Also, the AgF/PVP conductive tracks show an impressive transient performance, that the AgF/PVP tracks are dissolved in water within only 3 minutes. The applications of the transient AgF/PVP composite track in a LED circuit and dipole antenna demonstrate its potential in transient electronics. To achieve applications in implantable or wearable devices, the AgF/PVP conductive tracks will be printed on flexible substrates and encapsulated to avoid humility in the environment. We hope the work can promote the development of the transient electronic.

Conflicts of interest

The authors declare that they have no conflict of interest.

Acknowledgements

The authors are grateful for financial support from the National Natural Science Foundation of China (Grant No. 51705115). The authors declare that they have no conflict of interest.

References

1 B. H. Robinson, *Sci. Total Environ.*, 2009, **408**, 183–191.
2 L. H. Yamane, V. T. de Moraes, D. C. R. Espinosa and J. A. S. Tenório, *Waste Manag.*, 2011, **31**, 2553–2558.
3 K. K. Fu, Z. Wang, J. Dai, M. Carter and L. Hu, *Chem. Mater.*, 2016, **28**, 3527–3539.
4 R. Li, L. Wang, D. Kong and L. Yin, *Bioact. Mater.*, 2018, **3**, 322–333.
5 H. Cheng, *J. Mater. Res.*, 2016, **31**, 2549–2570.
6 S.-W. Hwang, D.-H. Kim, H. Tao, T.-i. Kim, S. Kim, K. J. Yu, B. Panilaitis, J.-W. Jeong, J.-K. Song, F. G. Omenetto and J. A. Rogers, *Adv. Funct. Mater.*, 2013, **23**, 4087–4093.
7 R. Widmer, H. Oswald-Krapf, D. Sinha-Khetriwal, M. Schnellmann and H. Boni, *Environ. Impact Assess. Rev.*, 2005, **25**, 436–458.
8 X. Tang, C. Shen, D. Shi, S. A. Cheema, M. I. Khan, C. Zhang and Y. Chen, *J. Hazard. Mater.*, 2010, **173**, 653–660.
9 Y. Chen, H. Lu, F. Xiu, T. Sun, Y. Ding, J. Liu and W. Huang, *Sci. Rep.*, 2018, **8**, 6408.
10 X. Huang, Y. Liu, S.-W. Hwang, S.-K. Kang, D. Patnaik, J. F. Cortes and J. A. Rogers, *Adv. Mater.*, 2014, **26**, 7371–7377.
11 S. K. Kang, G. Park, K. Kim, S. W. Hwang, H. Cheng, J. Shin, S. Chung, M. Kim, L. Yin, J. C. Lee, K. M. Lee and J. A. Rogers, *ACS Appl. Mater. Interfaces*, 2015, **7**, 9297–9305.
12 S. W. Hwang, S. K. Kang, X. Huang, M. A. Brenckle, F. G. Omenetto and J. A. Rogers, *Adv. Mater.*, 2015, **27**, 47–52.
13 S.-W. Hwang, G. Park, C. Edwards, E. A. Corbin, S.-K. Kang, H. Cheng, J.-K. Song, J.-H. Kim, S. Yu, J. Ng, J. E. Lee, J. Kim, C. Yee, B. Bhaduri, Y. Su, F. G. Omennetto, Y. Huang, R. Bashir, L. Goddard, G. Popescu, K.-M. Lee and J. A. Rogers, *ACS Nano*, 2014, **8**, 5843–5851.
14 G. A. Salvatore, J. Sülzle, F. Dalla Valle, G. Cantarella, F. Robotti, P. Jokic, S. Knobelspies, A. Daus, L. Büthe, L. Petti, N. Kirchgessner, R. Hopf, M. Magno and G. Tröster, *Adv. Funct. Mater.*, 2017, **27**, 1702390.
15 K. J. Yu, D. Kuzum, S. W. Hwang, B. H. Kim, H. Juul, N. H. Kim, S. M. Won, K. Chiang, M. Trumpis, A. G. Richardson, H. Cheng, H. Fang, M. Thomson, H. Bink, D. Talos, K. J. Seo, H. N. Lee, S. K. Kang, J. H. Kim, J. Y. Lee, Y. Huang, F. E. Jensen, M. A. Dichter, T. H. Lucas, J. Viventi, B. Litt and J. A. Rogers, *Nat. Mater.*, 2016, **15**, 782–791.
16 T. Lei, M. Guan, J. Liu, H. C. Lin, R. Pfattner, L. Shaw, A. F. McGuire, T. C. Huang, L. Shao, K. T. Cheng, J. B. Tok and Z. Bao, *Proc. Natl. Acad. Sci. U. S. A.*, 2017, **114**, 5107–5112.
17 L. Meng, S. M. Mahpeykar, Q. Xiong, B. Ahvazi and X. Wang, *RSC Adv.*, 2016, **6**, 85427–85433.
18 Y. Yang, K. Xu, T. Vervust and J. Vanfleteren, *Sens. Actuators, B*, 2018, **261**, 144–152.
19 Y. Yang, T. Vervust, S. Dunphy, S. Van Put, B. Vandecasteele, K. Dhaenens, L. Degrendele, L. Mader, L. De Vriese, T. Martens, M. Kaufmann, T. Sekitani and J. Vanfleteren, *Adv. Electron. Mater.*, 2018, **4**, 1800071.
20 Y. Yang, G. Chiesura, T. Vervust, F. Bossuyt, G. Luyckx, J. Degrieck and J. Vanfleteren, *Sens. Actuators, A*, 2016, **243**, 103–110.
21 A. Tuncuk, V. Stazi, A. Akcil, E. Y. Yazici and H. Deveci, *Miner. Eng.*, 2012, **25**, 28–37.
22 M. Goosey and R. Kellner, *Circuit World*, 2003, **29**, 33–37.
23 S. W. Hwang, H. Tao, D. H. Kim, H. Cheng, J. K. Song, E. Rill, M. A. Brenckle, B. Panilaitis, S. M. Won, Y. S. Kim, Y. M. Song, K. J. Yu, A. Ameen, R. Li, Y. Su, M. Yang, D. L. Kaplan, M. R. Zakin, M. J. Slepian, Y. Huang, F. G. Omenetto and J. A. Rogers, *Science*, 2012, **337**, 1640–1644.
24 L. Yin, H. Cheng, S. Mao, R. Haasch, Y. Liu, X. Xie, S.-W. Hwang, H. Jain, S.-K. Kang, Y. Su, R. Li, Y. Huang and J. A. Rogers, *Adv. Funct. Mater.*, 2014, **24**, 645–658.
25 D. R. Son, A. V. Raghu, K. R. Reddy and H. M. Jeong, *J. Macromol. Sci., Part B: Phys.*, 2016, **55**, 1099–1110.
26 K. R. Reddy, B. C. Sin, K. S. Ryu, J.-C. Kim, H. Chung and Y. Lee, *Synth. Met.*, 2009, **159**, 595–603.
27 K. R. Reddy, K. V. Karthik, S. B. B. Prasad, S. K. Soni, H. M. Jeong and A. V. Raghu, *Polyhedron*, 2016, **120**, 169–174.
28 M. Hassan, K. R. Reddy, E. Haque, S. N. Faisal, S. Ghasemi, A. I. Minett and V. G. Gomes, *Compos. Sci. Technol.*, 2014, **98**, 1–8.
29 S. H. Choi, D. H. Kim, A. V. Raghu, K. R. Reddy, H.-I. Lee, K. S. Yoon, H. M. Jeong and B. K. Kim, *J. Macromol. Sci., Part B: Phys.*, 2011, **51**, 197–207.
30 K. R. Reddy, K.-P. Lee and A. I. Gopalan, *J. Appl. Polym. Sci.*, 2007, **106**, 1181–1191.

Open Access Article. Published on 07 September 2020. Downloaded on 2/9/2026 7:46:54 PM.
This article is licensed under a Creative Commons Attribution-NonCommercial 3.0 Unported Licence.

31 K. R. Reddy, K.-P. Lee, Y. Lee and A. I. Gopalan, *Mater. Lett.*, 2008, **62**, 1815–1818.
32 K. R. Reddy, K. P. Lee and A. I. Gopalan, *J. Nanosci. Nanotechnol.*, 2007, **7**, 3117–3125.
33 H. M. H. Kakarla Raghava Reddy, Y. Lee and A. V. Raghu, *J. Polym. Sci., Part A: Polym. Chem.*, 2010, **48**, 1477–1484.
34 Y. R. Lee, S. C. Kim, H.-i. Lee, H. M. Jeong, A. V. Raghu, K. R. Reddy and B. K. Kim, *Macromol. Res.*, 2011, **19**, 66–71.
35 M. U. Khan, K. R. Reddy, T. Snguanwongchai, E. Haque and V. G. Gomes, *Colloid Polym. Sci.*, 2016, **294**, 1599–1610.
36 S. J. Han, H.-I. Lee, H. M. Jeong, B. K. Kim, A. V. Raghu and K. R. Reddy, *J. Macromol. Sci., Part B: Phys.*, 2014, **53**, 1193–1204.
37 M. B. Gebeyehu, Y. H. Chang, A. K. Abay, S. Y. Chang, J. Y. Lee, C. M. Wu, T. C. Chiang and R. I. Murakami, *RSC Adv.*, 2016, **6**, 54162–54168.
38 L. H. Tjeng, M. B. Meinders, J. van Elp, J. Ghijsen, G. A. Sawatzky and R. L. Johnson, *Phys. Rev. B: Condens. Matter Mater. Phys.*, 1990, **41**, 3190–3199.
39 J. F. Waver and G. B. Hoflund, *Chem. Mater.*, 1994, **6**, 1693–1699.
40 R. Jamshidi, S. Çinar, Y. Chen, N. Hashemi and R. Montazami, *J. Polym. Sci., Part B: Polym. Phys.*, 2015, **53**, 1603–1610.

 This journal is © The Royal Society of Chemistry 2020